Anatomy and histology of the foramen of ovarian bursa opening to the peritoneal cavity and its changes in autoimmune disease-prone mice

Short running: The foramen of ovarian bursa in mouse

Authors: Marina Hosotani[1*], Osamu Ichii[2, 3], Teppei Nakamura[2, 4], Takashi Namba[2], Md. Rashedul Islam[2], Yaser Hosny Ali Elewa[2, 5], Takafumi Watanabe[1], Hiromi Ueda[1], Yasuhiro Kon[2]

Addresses: [1] Laboratory of Veterinary Anatomy, Department of Veterinary Medicine, School of Veterinary Medicine, Rakuno Gakuen University, Ebetsu, Hokkaido 069-8501, Japan

[2]Laboratory of Anatomy, Department of Basic Veterinary Science, Faculty of Veterinary Medicine, Hokkaido University, Sapporo, Hokkaido 060-0818, Japan

[3]Laboratory of Agrobiomedical Science, Faculty of Agriculture, Hokkaido University, Sapporo, Hokkaido 060-0818, Japan

[4]Section of Biological Safety Research, Chitose Laboratory, Japan Food Research Laboratories, Chitose, Hokkaido 066-0052, Japan

[5]Department of Histology and Cytology, Faculty of Veterinary Medicine, Zagazig University, Zagazig 44519, Egypt

[*]Corresponding author: Marina Hosotani, DVM,

Laboratory of Veterinary Anatomy, Department of Veterinary Medicine, School of Veterinary Medicine, Rakuno Gakuen University,

Midorimachi 582, Bunkyodai, Ebetsu 069-8501, Japan.

20 Tel & Fax: +81-11-388-4763

21 Email: m-hosotani@rakuno.ac.jp

Abstract

The ovarian bursa is a small peritoneal cavity enclosed by the mesovarium and mesosalpinx, which surrounds the ovaries and oviductal infundibulum in mammals. The ovarian bursa is considered as the structure facilitating the transport of ovulated oocytes into the oviduct. Our previous study revealed reduced oocyte pick-up function in the oviduct of lupus-prone MRL/MpJ-Fas$^{lpr/lpr}$ mouse, suggesting the possibility of an escape of ovulated oocytes into the peritoneal cavity, despite the presence of an almost complete ovarian bursa in the mouse. In this study, we revealed anatomical and histological characteristics of the ovarian bursa in C57BL/6N, MRL/MpJ and MRL/MpJ-Fas$^{lpr/lpr}$ mice. All strains had the foramen of ovarian bursa (FOB), with a size of approximately 0.04 to 0.12 cm^2, surrounded by the ligament of ovarian bursa (LOB), which is part of the mesosalpinx. The LOB was partially lined with the cuboidal mesothelial cells and consisted of a thick smooth muscle layer in all strains. In 6-month-old MRL/MpJ-Fas$^{lpr/lpr}$ mice, in which the systemic autoimmune abnormality deteriorated and oocyte pick-up function was impaired, the size of the FOB tended to be larger than that of other strains. Additionally, in MRL/MpJ-Fas$^{lpr/lpr}$ mice at 6 months of age, there was infiltration by numerous immune cells in the mesosalpinx suspending the isthmus; however, the LOB prevented severe inflammation and showed deposition of collagen fibers. These results not only indicate that the FOB is a common structure within mice, but also imply the physiological function of the LOB and its role in maintenaning the microenvironment around the ovary, as well as regulating healthy reproduction.

Keywords: ovarian bursa; oviduct; mesosalpinx; 3D morphometry; reproduction

Introduction

The ovaries originate from the gonadal primordium, located in the lumbar region on the medial surface of mammalian mesonephros (König et al., 2009). Moreover, the oviducts and uterus develop from the Müllerian ducts (Yamamoto et al., 2018) and play crucial roles in female reproduction. The ovaries and oviducts are suspended within the mesovarium and mesosalpinx, respectively. These are the cranial parts of the broad ligament, ligamentum latum uteri, which is the common double-folded suspension of the mammalian female genital tract to the abdominal wall (König et al., 2009). The ovarian ligaments and the proper ligament of the ovary, ligamentum ovarii proprium, connect each ovary to the lateral side of the uterus (Craig and Billow, 2018). The mesovarium, mesosalpinx, and the proper ligament of the ovary enclose a small peritoneal cavity, termed the ovarian bursa, bursa ovarica, which surrounds the ovary and oviductal infundibulum (König et al., 2009).

The anatomical characteristics of the ovarian bursa, as well as ovulation rates, vary depending on the animal species. In cows, ovulation produces one oocyte at a time (Peters and McNatty, 1980), and the mesosalpinx surrounds the ovary like a mantle and forms a voluminous ovarian bursa with a wide cranio-ventromedial opening (Budras and Budras, 2003). In mares, ovulation produces one oocyte at a time (Ginther et al., 2001), and the ovary is too large to be located within the ovarian bursa (König et al., 2009). In female dogs, multiple ovulations produce about 5 to 7 oocytes at a time (Miranda et al., 2018), and the ovarian bursa completely encompasses the ovary within the foramen of ovarian bursa (FOB, *foramen bursae ovaricae*), which is a narrow slit-like opening to the peritoneal cavity (König et al., 2009). In mice, the ovulation rate is about eight at once, although the ovulation rate varies depending on the mice strain (Peters and McNatty, 1980); the ovaries are completely surrounded by

59 the ovarian bursa, which has a small peritoneal opening (Wimsatt and Waldo, 1945). Finally, female human have
60 no bursal structure around the ovaries (Beck, 1972; Ng and Barker, 2015).

61 The ovarian bursa is thought to play a role in preventing ovulated oocytes from escaping into the peritoneal
62 cavity, thus facilitating the transport of ovulated oocytes into the oviduct and assisting effective fertilization
63 (Zhang et al., 2013). Furthermore, surgical removal of the ovarian bursa surrounding the ovary of rodents leads
64 to a reduction in the number of oocytes picked-up by the oviductal infundibulum within the oviduct (Vanderhyden
65 et al., 1986; Kaufman et al., 2010). Based on the aforementioned anatomy and function of the murine ovarian
66 bursa, it has been suggested that the oocytes produced in the ovaries rarely escape into the peritoneal cavity in
67 mice.

68 In our previous work, we found that autoimmune disease-prone MRL/MpJ-*Fas*$^{lpr/lpr}$ (MRL/lpr) mice suffer a
69 reduction in oocyte pick-up by the oviductal infundibulum, resulting due to the progression of their systemic
70 autoimmune conditions (Hosotani et al., 2018). Furthermore, we showed that the ruptured follicles and corpora
71 hemorrhagica counts in whole-serial-sectioned ovaries, accounting for ovulated oocytes, exceeded the count of
72 cumulus-oocyte complexes in the oviductal ampulla picked up by the oviductal infundibulum of MRL/lpr mice
73 at 6 months of age with severe autoimmune abnormalities (Hosotani et al., 2018). This previous study unraveled
74 the possibility that the oocytes which progress into the ovarian bursa of mice are expelled into the peritoneal
75 cavity through the small peritoneal opening in the ovarian bursa. However, only a few anatomical and histological
76 studies of the murine ovarian bursa are available to confirm this hypothesis; hence, further investigations are
77 needed.

In the present study, we visualized and analyzed the structure of the ovarian bursa of three murine models: C57BL/6N (B6), MRL/MpJ (MRL/+), and MRL/lpr at 3 and 6 months of age. C57BL/6N (B6) is the most widely used of inbred mouse strain (Bryant, 2011), MRL/MpJ (MRL/+) is the parent and control strain for MRL/lpr (Heydemann, 2012), and the MRL/lpr strain is a systemic autoimmune disease-prone model which has an oocyte pick-up disorder, whose disease deteriorates at 6 months of age compared to 3 months of age (Hosotani et al., 2018). We found that all strains had the FOB within the mesosalpinx connecting oviduct and uterus. We also report the histological characteristics of the mesosalpinx surrounding the FOB, which is named the ligament of FOB (LOB). Moreover, we show that the LOB differs from other parts of the mesosalpinx, as the LOB is partially lined with cuboidal mesothelial cells and consists of a thick smooth muscle layer in all strains. In 6-month-old MRL/lpr mice with severe autoimmune disease, although the LOB prevented the infiltration of immune cells, it showed fibrosis; moreover, the FOB size in some of these mice was markedly larger than that of other strains and 3-month-old MRL/lpr mice. The results of our study provide insight on the anatomy, histology, reproductive biology, and experimental technology of the mouse.

Materials and Methods

Animals

Animal experimentation was approved by the Institutional Animal Care and Use Committee of the Graduate School of Veterinary Medicine, Hokkaido University (Approval No.15-0079), and the School of Veterinary Medicine, Rakuno Gakuen University (Approval No. VH19A6). Animals were handled in accordance with the

Guide for the Care and Use of Laboratory Animals, Graduate School of Veterinary Medicine, Hokkaido University, Japan (approved by the Association for Assessment and Accreditation of Laboratory Animal Care International), and with the Guide for the Care and Use of Laboratory Animals, Rakuno Gakuen University, Japan. Female B6, MRL/+, and MRL/lpr mice at 3 and 6 months of age were obtained from Japan SLC, Inc. (Hamamatsu, Shizuoka, Japan). Previous studies reported that autoimmune disease is severely exacerbated in female MRL/lpr mice at 6 months of age compared to its severity at 3 months of age (Hosotani et al., 2018, 2020). The mice were housed in groups within plastic cages at 18 - 26°C, under a 12 h light/dark cycle and had free access to a commercial diet and water. The estrous cycle of each mouse was confirmed by monitoring vaginal smears. All mice were euthanized by either severing of carotid artery or cervical dislocation, under deep anesthesia using a mixture of medetomidine (0.3 mg/kg), midazolam (4 mg/kg), and butorphanol (5 mg/kg). The spleen was collected from mice and the weight was measured.

Stereomicroscopical and histological observation of mice female reproductive tract

The female reproductive tract, including ovaries, oviducts, and a cranial part of the uterus were collected from mice. The morphology of these organs were kept in 0.01M phosphate buffered saline (PBS) and were observed under a stereo microscope. After observation, the organs were fixed with 4% paraformaldehyde (PFA) at 4°C overnight, embedded in paraffin, and cut into 3 μm-thick sections for immunohistochemistry and Masson's trichrome staining (MT) investigations.

India ink injection into the ovarian bursa

The female reproductive tract, including ovaries, oviducts, and a cranial part of the uterus, were collected from mice. A total of 10 to 20 µl India ink was injected into the ovarian bursa by inserting a glass capillary or 35 gauge needles, and the leakage of India ink through the FOB was observed.

Ultrastructural analysis of mice female reproductive tract

The female reproductive tract, including ovaries, oviducts, and a cranial part of the uterus were removed from mice during the estrus cycle and fixed using a fixing solution, containing 2.5% glutaraldehyde and 2% PFA. After six washes in 0.1 M phosphate buffer (PB), these organs were post-fixed with 1% osmium tetroxide in 0.1 M PB for 2 h at room temperature. After six washes in distilled water, the specimens were subjected to conductive treatment by 5% BEL-1 (Nisshin EM Co. Ltd., Tokyo, Japan) in 70% ethanol for 2 h at room temperature. Specimens were dried completely and examined using a S-2460N scanning electron microscope (Hitachi, Tokyo, Japan). Samples were sputter coated with gold using the ion-sputter E102 (Hitachi, Tokyo, Japan).

Area measurement of the opening of ovarian bursa reconstructed three-dimensionally

The ovaries, oviducts and the cranial part of the uterus were collected from mice during estrus. These organs were fixed with 4% PFA and kept at 4°C overnight. They were then embedded in paraffin and cut into 12 µm-thick whole serial sections. The serial hematoxylin and eosin-stained sections were used for both the histological observation and the three-dimensional (3D) reconstruction of the female reproductive organs. The 3D

reconstruction was processed using Fiji software, which is an image processing package of ImageJ (National Institutes of Health, Bethesda, Maryland, USA), and Image Pro software (Media Cybernetics Inc., Rockville, Maryland, USA). The alignment of each pictured section in whole serial sections was adjusted by the Register Virtual Stack Slices plugin provided in Fiji (National Institutes of Health, Bethesda, Maryland, USA). Based on these aligned 2D pictures of the female reproductive tract, 3D geometrical models of female reproductive tracts were created using the Image Pro software (Media Cybernetics Inc., Rockville, Maryland, USA). The peritoneal side of the FOB observed in these 3D models was measured using Image Pro software (Media Cybernetics Inc., Rockville, Maryland, USA).

Immunohistochemistry

The 3 μm-thick sections of female reproductive organs of mice during estrus were incubated in 20 mM tris-HCl (pH 9.0) (for B220, B cell marker; CD3, T cell marker; Foxp3, regulatory T cell marker), or 10 mM citrate buffer (pH 6.0) (for Iba1, macrophage marker; Lyve1, lymphatic vessel marker; alpha smooth muscle actin (αSMA), smooth muscle cell marker) for 15 min at 110°C. Sections were then soaked in methanol, containing 0.3% hydrogen peroxide (H_2O_2). Sections that were blocked using 10% normal goat serum for 60 min at room temperature were incubated at 4°C overnight with rat anti-B220 (1:1600, Cedarlane, Ontario, Canada), rabbit anti-CD3 (ready to use, Nichirei Bioscience Inc., Tokyo, Japan), rabbit anti-Iba1 (1:1200, FUJIFILM Wako Pure Chemical Co., Ltd., Osaka, Japan), rat anti-Foxp3 (1:100, Thermo Fisher Scientific K.K., Tokyo, Japan), rabbit anti-Lyve1 (1:500, AdipoGen Inc., San Diego, California, USA) or rabbit anti-αSMA (1:3000, Abcam CO.,

Cambridge, UK). After three washes in 0.01 M PBS, sections were incubated with biotin-conjugated goat anti-rabbit IgG (SABPRO Kit, Nichirei Bioscience Inc.), or goat anti-rat IgG antibody (1:150, BioLegend Inc., San Diego, California, USA) for 30 min, and washed and incubated for 30 min at room temperature, using a streptavidin-biotin complex (SABPRO Kit, Nichirei Bioscience Inc.). Sections were then incubated with 3, 3′ – diaminobenzidine tetrahydrochloride-H_2O_2 solution, and lightly stained with hematoxylin.

Statistical analysis

Results were expressed as mean ± standard error of the mean (SEM) and statistically analyzed in a non-parametric manner. Two groups were compared using the Mann-Whitney *U*-test ($P < 0.05$). The Kruskal-Wallis test was used to compare the three groups; multiple comparisons were performed using Scheffé's method when significant differences were observed ($P < 0.05$).

Results

The morphology of the peritoneal opening of the ovarian bursa of mice

Under the stereomicroscope, it was found that there is common positional anatomy of the female reproductive tract among the three strains at both ages, and both the left and right ovaries were located on the cranial side of the oviducts, folded like a coil connecting to the uterus (Figure 1). Most parts of the ovaries in all mice were covered by continuous mesovarium and mesosalpinx. Notably, MRL/+ mice at 6 months of age developed ovarian cysts (Figure 1) (Kon et al., 2007). In the magnified stereomicroscopical observations, the

oviducts folded like a coil by the mesosalpinx were clearly observed in the female reproductive tract of all strains. The coiled oviducts were connected to the cranial part of the uterus by the mesosalpinx, which surrounded the slit-shaped peritoneal openings in the ovarian bursa. Both the left and right ovaries had peritoneal openings generally less than 1 mm in length, which were commonly observed at the same position of the female reproductive tract of all strains at both ages. The slit-shaped peritoneal opening in the ovarian bursa of the mouse is named the FOB, based on the anatomical vocabulary of the narrow slit-like opening observed in the ovarian bursa of female dogs (König et al., 2009). The mesosalpinx surrounding the murine FOB is named the LOB (ligament of ovarian bursa). Some, but not all, of the ovarian bursa of the 6-month-old MRL/lpr mice exhibited a larger FOB than that of other individuals. Furthermore, the oviductal infundibulum enclosed the ovarian bursa and was observed from the peritoneal side, as shown in the FOB of the right side ovaries of MRL/lpr mice at 6 months of age in Figure 1. The India ink injected into the ovarian bursa leaked through the FOB in the three strains at both ages (Figure 2 and Supplementary Movie S1).

The ultrastructure of FOB was also observed in all strains (Figure 3). As shown through stereomicroscopical observations, the FOB in mice was surrounded by the LOB, which was slit-shaped or had a slightly expanded ellipsoid shape. Furthermore, mesothelial cells lining the LOB in B6 and MRL/+ mice exhibited spherical dome like morphology (Figure 3, arrowheads in insets). In MRL/lpr mice, the mesothelium of the LOB had a deeply tangled surface. The ultrastructural differences of the FOB between the left and right sides were not observed.

The female reproductive tract reconstructed in 3D by superimposing the images of their whole serial sections reproduced the morphology of the FOB in the mesothelium (Figure 4A). Furthermore, we measured the

peritoneal side area of the FOB (Figure 4B). Although the area had no significant differences among strains at both 3 and 6 months of age, MRL/lpr mice at 6 months of age tended to have a larger FOB size than other strains at the same age.

The histology of the LOB of mice

The presence of the FOB in all strains was confirmed in the histological sections shown in Figure 5. The whole serial sections of the female reproductive tract of mice revealed that the ovarian bursa did not have apertures that were continuous with the peritoneal cavity, other than the FOB (data not shown). This histological observation also showed that the FOB was surrounded by the LOB connecting the isthmus or ampulla of the oviducts and the cranial part of the uterus. The epithelium of the LOB facing the FOB was lined with mesothelial cells, which were, in part, cuboidal epithelial cells (Figure 5). Significant histological differences in the LOB were not observed among the strains at both 3 and 6 months of age and the left and right sides.

The distribution of smooth muscle cells and collagen fibers in the LOB of mice

Immunohistochemical analysis identified smooth muscle cells as the cell types that compose the connective tissue under the epithelium of the LOB (Figure 6). To examine the distribution of the collagen fibers in the LOB, MT staining was performed (Figure 6, MT). In the LOB of B6 mice at both 3 and 6 months of age, the thick collagen fibers were distributed underneath the mesothelium and between smooth muscle layers (Figure 6). In the LOB of MRL/+ mice at 3 and 6 months of age, as well as in MRL/lpr mice at 3 months of age, the distribution of

thick collagen fibers was not significant. However, it was observed that the thick and dense aniline blue^{+} collagen fibers were distributed underneath the mesothelium and partially between the smooth muscle layers in the LOB of MRL/lpr mice, at 6 months of age (Figure 6).

The distribution of immune cells in the LOB of mice

MRL/lpr mouse is well known as a severe systemic autoimmune disease model (Kamogawa et al., 2002). The severe inflammation of immune cells affects ovaries and the oviduct of MRL/lpr mice at 6 months of age (Otani et al., 2015; Hosotani et al., 2018). In this study, we confirmed that MRL/lpr mice showed more significant splenomegaly at 3 and 6 months of age compared to that of other strains. We also showed that the splenomegaly in MRL/lpr mice was exacerbated at 6 months of age (Supplementary Figure S2). To examine the effect of the inflammation in the LOB of the mice, we performed immunohistochemistry to detect B cells, T cells, macrophages, and regulatory T cells. In the mesosalpinx folding the isthmus, there was significant infiltration of immune cells, including B220^{+} B cells, CD3^{+} T cells, and Iba1^{+} macrophages (Figure 7). In MRL/lpr mice at both 3 and 6 months, compared to the other strains, a larger distribution of Foxp3^{+} regulatory T cells was observed (Figure 7). The infiltration of the immune cells was more profound in MRL/lpr mice at 6 months of age than at 3 months of age. However, no significant distribution of B220^{+} B cells, CD3^{+} T cells, Iba1^{+} macrophages, or Foxp3^{+} regulatory T cells in the LOB was observed in any of the mice used in this study (Figure 8). The lymphatic vessels, visualized by the Lyve1 positive reaction, were distributed directly underneath the LOB, as well as in the connective tissue of the LOB, in all strains at 3 and 6 months of age. The number of these immune cells and

lymphatic vessels in the LOB exhibited no differences among the strains at 3 and 6 months of age.

Discussion

Over 70 years ago, Wimsatt and his colleagues reported for the first time that a peritoneal opening generally appears in the ovarian bursa of B6 and Swiss strain of mice (Wimsatt and Waldo, 1945). However, the rather small morphology of the FOB, which is rarely observed in the histological section of female reproductive tracts, led to misinterpretations in several reports which stated that mice have a complete ovarian bursa with no peritoneal opening, with completely enveloped ovaries (Beck, 1972; Cotchin and Marchant, 1977a, 1977b; Kaufman et al., 2010; Dixon et al., 2014). This study confirmed and revealed that both B6 and MRL-background strains of mice have peritoneal openings in the ovarian bursa, indicating that the FOB surrounded by the LOB, which connects the oviduct and the cranial part of the uterus, is the general female reproductive structure in mice (Figure 9). As for other rodents, rats also have a small opening in the ovarian bursa to the peritoneal cavity (Kellogg, 1941). However, in golden hamsters, each ovary has been reported to be enclosed within a complete bursa that is connected with the oviduct (Cotchin and Marchant, 1977b; Martin et al., 1981; Shinohara et al., 1987). Interestingly, the monotocous species possess neither a bursa (as in the case of the female human) nor an ovarian bursa that is strongly connected with the peritoneal cavity (as in the cases of the mare and cow), but polytocous species possess an almost complete ovarian bursa (as in the cases of the rodents) (Kaufman et al., 2010). The anatomical characteristics of the mammalian ovarian bursa can provide key information to explain the biological and evolutional differences in their reproduction.

The almost closed appearance of the murine ovarian bursa has been used for the intrabursal injection technique, which is a method of topical drug delivery to ovaries by the injection of a solution into the bursal cavity of an anesthetized animal (Martin et al., 1981; Van der Hoek et al., 2000). It is also used as the method for selective introduction of genetic information to alter the ovarian surface epithelium (Clark-Knowles et al., 2007; Kaufman et al., 2010). However, it has been suggested that the ovarian bursa may play an active role in regulating local fluid homeostasis during the ovulation (Zhang et al., 2013). The intrabursal fluid interchange is thought to be bidirectional between the peritoneal cavity and the reproductive tract through the FOB. This rationale is based on the observation that particles of india ink, which was injected into the peritoneal cavity of mice, were found to be abundantly present in the ovarian bursa and oviduct during the ovulation period (Wimsatt and Waldo, 1945). Although we examined the FOB and LOB of the mice at estrus in this study, further studies using mice at various stages in the estrous cycle can help to reveal additional morphological differences between the FOB and LOB. Furthermore, we found that the LOB possesses a thick, smooth muscle layer, which indicates that the FOB alters its area depending on the physiological, hormonal, and pathological conditions of the female reproductive tract by contracting the LOB. Therefore, in order to get accurate results, the selection of an optimal injection time, while taking into consideration the stage of the estrous cycle and/or light-dark cycle, as well as the consistency of the injection timing through a series of experiments is important for researchers who perform intrabursal injections.

The ovarian bursa is a key player in maintaining an adaptive ovarian microenvironment for ovulation (Li et al., 2007). Lymphatic stomata are small openings in lymphatic capillaries on the free surface of the mesothelium

(Wang et al., 2010). The ovarian bursa of the golden hamster has lymphatic stomata that connects the bursal cavity with the lymphatic lumen (Shinohara et al., 1987). It is suggested that the opening area of lymphatic stomata varies under different fluid pressure and mechanical forces (Li et al., 2007). In addition to these theories, the muscular structure of the LOB surrounding the FOB provides us with a novel hypothesis that the contraction of the FOB also plays a role in maintaining the bursal liquid and/or hormonal homeostasis, by discarding the bursal liquid into the peritoneal cavity.

The peritoneum is composed of an extensive squamous or cuboidal monolayer of mesothelial cells that rests on the fibrous connective tissue underneath (Yung et al., 2006; Isaza-Restrepo et al., 2018). The cuboidal mesothelial cells appear in the septal folds of the mediastinal pleura, liver, and spleen, and are in a metabolically active state (Mutsaers, 2002). The peritoneum facilitates immune induction, modulation, and inhibition, as the mesothelial cells are capable of recognizing pathogens and tissue damage, and initiating inflammatory responses through antigen presentation, cytokine production, and interaction with immune cells, such as macrophages (Isaza-Restrepo et al., 2018). In swine, mesothelial cells covering the ovarian bursa are cuboidal and biosynthetically activated, which suggests that these mesothelial cells may produce large amounts of surfactants and regulate immunomodulation, fluid balance, lubrication, and protection (Yániz et al., 2007). We report that the epithelium of the LOB in mice is partially lined with such cuboidal mesothelial cells. Hence, the LOB might have the unique function to regulate intrabursal immune balance and thereby promote healthy reproductive processes in the ovary. Previous studies reported that autoimmune disease in female MRL/lpr mice is severely exacerbated at 6 months of age, and the severe inflammation due to the infiltration of immune cells affects the ovaries and

287 oviduct (Otani et al., 2015; Hosotani et al., 2018). In this study, the lymphoma-like infiltration of inflammatory
288 cells, including B cells, T cells, and macrophages was observed in the mesosalpinx folding the isthmus in MRL/lpr
289 mice at 6 months of age. However, this was not observed in the LOB, thereby suggesting a higher ability of the
290 LOB to regulate immune conditions compared to typical mesosalpinx. Further investigations will be needed to
291 confirm these hypotheses.

292 Notably, the MRL/lpr at 6 months of age with severe autoimmune conditions lose their ovulated oocytes into
293 the coeloma, which is neither the ovarian bursa nor the oviductal lumen (Hosotani et al., 2018). The diameter of
294 mouse oocytes is approximately 80 μm (Xiao et al., 2015). Based on our findings that the area of FOB in mice
295 was approximately 0.04 to 0.12 cm^2, and given smooth muscle contraction in the LOB might change the area of
296 the FOB, we hypothesise that the oocytes released from the ovaries into the ovarian bursa can escape into the
297 peritoneal cavity through the FOB in mice with autoimmune issues. In MRL/lpr mice in the severe disease stage,
298 some of which possessed larger than average FOB relative to other strains and individuals, the altered morphology
299 and function of the FOB might be one of the causes for the dysfunction of oocyte pick-up, in addition to the
300 inflammation and abnormal morphology in the oviductal infundibulum (Hosotani et al., 2018).

301 The chronic inflammatory reactions triggered by persistent infections, autoimmune reactions, allergic
302 responses, and tissue injury result in fibrosis (Wynn, 2008). In addition organs such as lungs, heart, liver, kidney,
303 intestine, and skin (Wynn, 2008), the peritoneum is also pathologically affected by chronic inflammation and
304 fibrosis (Wang et al., 2016). Even in MRL/lpr mice at 6 months of age which have severe inflammation in the
305 mesosalpinx, there were only a small number of immune cells infiltrating the LOB. Nonetheless, the inflammation

enhances fibrosis in the LOB in MRL/lpr mice at 6 months of age, compared to 3 months of age, and MRL/+ at both ages. Once initiated, fibrogenesis in the intestine is no longer dependent on the presence of inflammation, suggesting that the fibrosis is self-propagating (Johnson et al., 2012). Although inflammation is prerequisite for the initiation of fibrosis, the severity of inflammation during fibrogenesis does not correlate with the degree of collagen deposition (Hünerwadel et al., 2018). Therefore, we consider that the severe and chronic systemic immune abnormalities, which deteriorate in the later life of MRL/lpr mice, alter the hormonal environment post-ovulation and immunological microenvironment, including cytokines in female reproductive organs. This leads to the deposition of thick collagen fibers in MRL/lpr mice at 6 months of age. The ultrastructure of the surface of the LOB revealed highly complicated LOB in MRL/lpr mice, which corresponds with the histological observation of thick collagen deposition underneath the mesothelium. Although it is unclear whether fibrosis affects the function of the LOB and morphology of the FOB, considering that B6 mice also possess the fibrotic LOB at both 3 and 6 months of age, the deposition of collagen fibers in MRL/lpr mice in the severe disease stage might make the LOB stiffer than at younger ages. This can occur as organs increase their extracellular matrix, which contains fibrillar collagens (Wells, 2013), thus resulting in a stiffer LOB. Repeated ovulation induces an acute pro-inflammatory environment on the ovarian surface and oviductal fimbria, increasing ovarian cancer risk (Trabert et al., 2020). Although the ovulation rate of C57BL/6 and MRL strain mice is similar (about 10 oocytes per estrus) (Hosotani et al., 2019), the impaired clearance of intrabrusal fluid containing inflammatory substances derived from ovarian follicles would cause pathology not only of the ovaries but also of the oviducts. The stiffer LOB perhaps affects the ovarian pathology due to impaired bursal fluid regulation in mice.

In conclusion, the ovarian bursa of mouse is connected to the peritoneal cavity, which is a characteristic similar to those of other mammals, such as ruminants and horses. We have also reported the physiological function of the LOB with a thick, smooth muscle layer in the maintenance of the fluid microenvironment and immune condition around the ovary. Further studies on the function of the FOB will provide a novel reproductive theory on maintenance of healthy ovulation and oocyte-pick-up by the oviductal infundibulum by regulating intraovarian bursal homeostasis.

Acknowledgements

This work was supported in part by JSPS KAKENHI (No. JP18J22313, 19K23708) and Rakuno Gakuen University Research Fund (No. 2020-01) (M. Hosotani). The research described in this paper was presented in part at the 162th Japanese Association of Veterinary Anatomists, 10-12 September 2019 in Ibaraki.

Author contributions

M. Hosotani designed and performed experiments, as well as analyzed the data. T. Namba performed the sampling of mice. O. Ichii, T. Nakamura, Y.H.A. Elewa and Y. Kon designed and reviewed the experiments. M. Hosotani, O. Ichii and Y. Kon wrote the manuscript. M. I. Rashedul, T. Watanabe, H. Ueda reviewed the manuscript. All authors approved the final manuscript.

Conflicts of Interest

The authors declare no conflicts of interest.

Data availability statement

The data that support the findings of this study are available from the corresponding author upon reasonable request.

References

Beck, L. R. (1972). Comparative observations on the morphology of the mammalian periovarial sac. *J. Morphol.* 136, 247–254. doi:10.1002/jmor.1051360208.

Bryant, C. D. (2011). The blessings and curses of C57BL/6 substrains in mouse genetic studies. *Ann. N. Y. Acad. Sci.* 1245, 31–33. doi:10.1111/j.1749-6632.2011.06325.x.

Budras, K.-D., and Budras, K.-D. (2003). *Bovine Anatomy: An Illustrated Text*. First Edit. Hannover, Germany: Schlütersche, pp. 86.

Clark-Knowles, K. V., Garson, K., Jonkers, J., and Vanderhyden, B. C. (2007). Conditional inactivation of Brca1 in the mouse ovarian surface epithelium results in an increase in preneoplastic changes. *Exp. Cell Res.* 313, 133–145. doi:10.1016/j.yexcr.2006.09.026.

Cotchin, E., and Marchant, J. (1977a). “Animal models for tumors of the ovary and uterus.,” in *Animal tumors of the female reproductive tract* . New York, USA: Springer New York, pp. 1–25.

Cotchin, E., and Marchant, J. (1977b). "Spontaneous tumors of the uterus and ovaries in animals.” in *Animal tumors of the female reproductive tract* . New York, USA: Springer New York.

Craig, M. E., and Billow, M. (2018). *Anatomy, Abdomen and Pelvis, Broad Ligaments*. Available at: http://www.ncbi.nlm.nih.gov/pubmed/29763118 [Accessed November 12, 2019].

Dixon, D., Alison, R., Bach, U., Colman, K., Foley, G. L., Harleman, J. H., et al. (2014). Nonproliferative and proliferative lesions of the rat and mouse female reproductive system. *J. Toxicol. Pathol.* 27. doi:10.1293/tox.27.1S.

Ginther, O. J., Beg, M. A., Bergfelt, D. R., Donadeu, F. X., and Kot, K. (2001). Follicle Selection in Monovular Species. *Biol. Reprod.* 65, 638–647. doi:10.1095/biolreprod65.3.638.

Heydemann, A. (2012). The super super-healing MRL mouse strain. *Front. Biol. (Beijing).* 7, 522–538. doi:10.1007/s11515-012-1192-4.

Hosotani, M., Ichii, O., Nakamura, T., Kanazawa, S. O., Elewa, Y. H. A., and Kon, Y. (2018). Autoimmune abnormality affects ovulation and oocyte-pick-up in MRL/MpJ-Fas lpr/lpr mice. *Lupus* 27, 82–94. doi:10.1177/0961203317711772.

Hosotani, M., Ichii, O., Nakamura, T., Masum, M. A., Otani, Y., Elewa, Y. H. A., et al. (2020). Altered ciliary morphofunction in the oviductal infundibulum of systemic autoimmune disease-prone MRL/MpJ-Fas lpr/lpr mice. *Cell Tissue Res.* doi:10.1007/s00441-020-03175-z.

Hosotani, M., Ichii, O., Nakamura, T., Masum, M. A., Otani, Y., Otsuka-Kanazawa, S., et al. (2019). MRL/MpJ mice produce more oocytes and exhibit impaired fertilisation and accelerated luteinisation after superovulation treatment. *Reprod. Fertil. Dev.* 31, 760. doi:10.1071/RD18319.

Hünerwadel, A., Fagagnini, S., Rogler, G., Lutz, C., Jaeger, S. U., Mamie, C., et al. (2018). Severity of local inflammation does not impact development of fibrosis in mouse models of intestinal fibrosis. *Sci. Rep.* 8. doi:10.1038/s41598-018-33452-5.

Isaza-Restrepo, A., Martin-Saavedra, J. S., Velez-Leal, J. L., Vargas-Barato, F., and Riveros-Dueñas, R. (2018). The peritoneum: Beyond the tissue - A review. *Front. Physiol.* 9. doi:10.3389/fphys.2018.00738.

Johnson, L. A., Luke, A., Sauder, K., Moons, D. S., Horowitz, J. C., and Higgins, P. D. R. (2012). Intestinal

fibrosis is reduced by early elimination of inflammation in a mouse model of IBD: Impact of a “Top-Down” approach to intestinal fibrosis in mice. *Inflamm. Bowel Dis.* 18, 460–471. doi:10.1002/ibd.21812.

Kamogawa, J., Terada, M., Mizuki, S., Nishihara, M., Yamamoto, H., Mori, S., et al. (2002). Arthritis in MRL/lpr mice is under the control of multiple gene loci with an allelic combination derived from the original inbred strains. *Arthritis Rheum.* 46, 1067–1074. doi:10.1002/art.10193.

Kaufman, M. H., Nikitin, A. Y., and Sundberg, J. P. (2010). "Histologic Basis of Mouse Endocrine System Development" in *A Comparative Analysis*. First Edition. Florida, USA: CRC Press, pp. 190.

Kellogg, M. P. (1941). The development of the periovarial sac in the white rat. *Anat. Rec.* 79, 465–477. doi:10.1002/ar.1090790406.

Kon, Y., Konno, A., Hashimoto, Y., and Endoh, D. (2007). Ovarian cysts in MRL/MpJ mice originate from rete ovarii. *Anat. Histol. Embryol.* 36, 172–178. doi:10.1111/j.1439-0264.2006.00728.x.

König, H. E., Liebich, H.-G., and Bragulla, H. (2009). *Veterinary anatomy of domestic mammals : textbook and colour atlas*. 4th Edition. Stuttgart, Germany: Schattauer Verlag, pp. 423, 429-30.

Li, M., Zhou, T. H., Gao, Y., Zhang, N., and Li, J. C. (2007). Ultrastructure and estrogen regulation of the lymphatic stomata of ovarian bursa in mice. *Anat. Rec.* 290, 1195–1202. doi:10.1002/ar.20583.

Martin, G. G., Talbot, P., and Pendergrass, P. (1981). An intrabursal injection procedure for the in vivo study of ovulation in hamsters. *J. Exp. Zool.* 216, 461–468. doi:10.1002/jez.1402160315.

Miranda, S., Carolino, N., Vilhena, H., Payan-Carreira, R., and Pereira, R. M. L. N. (2018). Early embryo development, number, quality, and location and the relationship with plasma progesterone in dogs. *Anim.*

406 *Reprod. Sci.* 198, 238–245. doi:10.1016/j.anireprosci.2018.10.001.

407 Mutsaers, S. E. (2002). Mesothelial cells: Their structure, function and role in serosal repair. *Respirology* 7,

408 171–191. doi:10.1046/j.1440-1843.2002.00404.x.

409 Ng, A., and Barker, N. (2015). Ovary and fimbrial stem cells: Biology, niche and cancer origins. *Nat. Rev. Mol.*

410 *Cell Biol.* 16, 625–638. doi:10.1038/nrm4056.

411 Otani, Y., Ichii, O., Otsuka-Kanazawa, S., Chihara, M., Nakamura, T., and Kon, Y. (2015). MRL/MpJ- *Fas* ^{lpr}

412 mice show abnormalities in ovarian function and morphology with the progression of autoimmune disease.

413 *Autoimmunity* 48, 402–411. doi:10.3109/08916934.2015.1031889.

414 Peters, H., and McNatty, K. P. (1980). *The ovary : a correlation of structure and function in mammals*.

415 Berkeley, California: University of California Press. pp. 75.

416 Shinohara, H., Nakatani, T., and Matsuda, T. (1987). Postnatal development of the ovarian bursa of the golden

417 hamster (Mesocricetus auratus): Its complete closure and morphogenesis of lymphatic stomata. *Am. J.*

418 *Anat.* 179, 385–402. doi:10.1002/aja.1001790408.

419 Trabert, B., Tworoger, S. S., O'Brien, K. M., Townsend, M. K., Fortner, R. T., Iversen, E. S., et al. (2020). The

420 risk of ovarian cancer increases with an increase in the lifetime number of ovulatory cycles: An analysis

421 from the Ovarian Cancer Cohort Consortium (OC3). *Cancer Res.* 80, 1210–1218. doi:10.1158/0008-

422 5472.CAN-19-2850.

423 Van der Hoek, K. H., Maddocks, S., Woodhouse, C. M., van Rooijen, N., Robertson, S. A., and Norman, R. J.

424 (2000). Intrabursal Injection of Clodronate Liposomes Causes Macrophage Depletion and Inhibits

425 Ovulation in the Mouse Ovary1. *Biol. Reprod.* 62, 1059–1066. doi:10.1095/biolreprod62.4.1059.

426 Vanderhyden, B. C., Rouleau, A., and Armstrong, D. T. (1986). Effect of removal of the ovarian bursa of the rat

427 on infundibular retrieval and subsequent development of ovulated oocytes. *Reproduction* 77, 393–399.

428 doi:10.1530/jrf.0.0770393.

429 Wang, L., Liu, N., Xiong, C., Xu, L., Shi, Y., Qiu, A., et al. (2016). Inhibition of EGF receptor blocks the

430 development and progression of peritoneal fibrosis. *J. Am. Soc. Nephrol.* 27, 2631–2644.

431 doi:10.1681/ASN.2015030299.

432 Wang, Z.-B., Li, M., and Li, J.-C. (2010). Recent Advances in the Research of Lymphatic Stomata. *Anat. Rec.*

433 *Adv. Integr. Anat. Evol. Biol.* 293, 754–761. doi:10.1002/ar.21101.

434 Wells, R. G. (2013). Tissue mechanics and fibrosis. *Biochim. Biophys. Acta - Mol. Basis Dis.* 1832, 884–890.

435 doi:10.1016/j.bbadis.2013.02.007.

436 Wimsatt, W. A., and Waldo, C. M. (1945). The normal occurrence of a peritoneal opening in the bursa ovarii of

437 the mouse. *Anat. Rec.* 93, 47–57. doi:10.1002/ar.1090930105.

438 Wynn, T. A. (2008). Cellular and molecular mechanisms of fibrosis. *J. Pathol.* 214, 199–210.

439 doi:10.1002/path.2277.

440 Xiao, S., Duncan, F. E., Bai, L., Nguyen, C. T., Shea, L. D., and Woodruff, T. K. (2015). Size-specific follicle

441 selection improves mouse oocyte reproductive outcomes. *Reproduction* 150, 183–192. doi:10.1530/REP-

442 15-0175.

443 Yamamoto, A., Omotehara, T., Miura, Y., Takada, T., Yoneda, N., Hirano, T., et al. (2018). The mechanisms

underlying the effects of amh on müllerian duct regression in male mice. *J. Vet. Med. Sci.* 80, 557–567. doi:10.1292/jvms.18-0023.

Yániz, J. L., Recreo, P., Carretero, T., Arceiz, E., Hunter, R. H. F., and López-Gatius, F. (2007). The Peritoneal Mesothelium Covering the Genital Tract and its Ligaments in the Female Pig Shows Signs of Active Function. *Anat. Rec. Adv. Integr. Anat. Evol. Biol.* 290, 831–837. doi:10.1002/ar.20554.

Yung, S., Li, F. K., and Chan, T. M. (2006). Peritoneal mesothelial cell culture and biology. *Perit. Dial. Int.* 26, 162–173.

Zhang, H., Zhang, Y., Zhao, H., Zhang, Y., Chen, Q., Peng, H., et al. (2013). Hormonal Regulation of Ovarian Bursa Fluid in Mice and Involvement of Aquaporins. *PLoS One* 8, e63823. doi:10.1371/journal.pone.0063823.

Figure legends

Figure 1. The stereomicroscopical morphology of the foramen of the ovarian bursa in mice.

Arrows show the positions of the foramen of the ovarian bursa. The squares surrounded by dashed lines are magnified in images on the right side. The line drawings in the insets imitate the shape of the foramen of the ovarian bursa. Asterisk shows the infundibulum enveloped in the ovarian bursa of MRL/lpr mice at 6 months of age.

L: left, R: right, O: ovary, T: oviduct, U: uterus, †: ovarian cyst. B6: C57BL/6N, MRL/+: MRL/MpJ, MRL/lpr: MRL/MpJ-Fas$^{lpr/lpr}$.

Figure 2. Leakage of India ink from the ovarian bursa to extrabursa through the foramen of the ovarian bursa in mice.

Arrows indicate the points where the India ink leaked (i.e., foramen of the ovarian bursa).

O: ovary, T: oviduct, U: uterus. B6: C57BL/6N, MRL/+: MRL/MpJ, MRL/lpr: MRL/MpJ-Fas$^{lpr/lpr}$.

Figure 3. The ultrastructure of the foramen of ovarian bursa in mice.

Arrowheads indicate the spherical dome like mesothelial cells lining the LOB.

T: oviduct, U: uterus, FOB: the foramen of ovarian bursa, LOB: the ligament of ovarian bursa. B6: C57BL/6N, MRL/+: MRL/MpJ, MRL/lpr: MRL/MpJ-Fas$^{lpr/lpr}$.

Figure 4. 3D reconstruction of the female reproductive tract and the size measurement of the foramen of ovarian bursa in mice.

(A) The mesothelium composing the female reproductive tract is colored in red. The foramen of ovarian bursa is colored in black and indicated by black arrowheads. The dashed yellow lines indicate the inside of the ovarian bursa, while the yellow arrows indicate the outside of the ovarian bursa. LOB: ligament of ovarian bursa, U: uterus.

(B) The peritoneal side area of the foramen of the ovarian bursa is measured. n = 4 per group. There is no significant strain-related difference in the same age examined by the Kruskal-Wallis test followed by Scheffé's method and no significant differences between 3 and 6 months of age in the same strain examined by the Mann-Whitney *U*-test. Data is presented as the mean ± SEM.

B6: C57BL/6N, MRL/+: MRL/MpJ, MRL/lpr: MRL/MpJ-Fas$^{lpr/lpr}$.

Figure 5. The histology of the foramen and ligament of ovarian bursa in mice.

The hematoxylin and eosin staining. The squares surrounded by black dashed lines are magnified in the images on the right side. The blue lines indicate the boundary of the ovarian bursa. Arrows connecting the intrabursal and peritoneal sides are passing through the foramen of the ovarian bursa, and the centers are indicated by asterisks. Arrowheads indicate the cuboidal mesothelial cells lining the epithelium of the foramen of ovarian bursa. A: ampulla, B: ovarian bursa, In: infundibulum, Is: isthmus, O: ovary, Out: ostium uterinum tubae, U: uterus. B6: C57BL/6N, MRL/+: MRL/MpJ, MRL/lpr: MRL/MpJ-Fas$^{lpr/lpr}$.

Figure 6. The distribution of smooth muscle cells and collagen fibers in the ligament of ovarian bursa in mice.

The squares surrounded by black dashed lines are magnified in the insets. Asterisks: the foramen of ovarian bursa, Arrows: thick collagen fibers in the ligament of ovarian bursa, αSMA: alpha smooth muscle actin, immunohistochemistry, MT: masson's trichrome staining. B6: C57BL/6N, MRL/+: MRL/MpJ, MRL/lpr: MRL/MpJ-Fas$^{lpr/lpr}$.

Figure 7. The immunohistochemistry of immune cells in the mesosalpinx suspending the oviductal isthmus in mice.

Black circles surround the area of severe infiltration of immune cells. The squares surrounded by the black dashed lines are magnified in the insets, showing the area of significant infiltration of the immune cells. Arrows indicate the distribution of the Foxp3 positive cells. Is: isthmus. B6: C57BL/6N, MRL/+: MRL/MpJ, MRL/lpr: MRL/MpJ-Fas$^{lpr/lpr}$.

Figure 8. The immunohistochemistry of immune cells in the ligament of ovarian bursa in mice.

Arrows indicate the distribution of immune cells in the connective tissue of the ligament of ovarian bursa. Asterisks: the foramen of ovarian bursa. B6: C57BL/6N, MRL/+: MRL/MpJ, MRL/lpr: MRL/MpJ-Fas$^{lpr/lpr}$.

Figure 9. The anatomical schema of the foramen and ligament of ovarian bursa.

The mesovarium and mesosalpinx enclose the peritoneal cavity, which is called the ovarian bursa, and the large part of ovary. The mesosalpinx connecting the oviductal ampulla or isthmus and the cranial part of uterus has the silt-like opening of the ovarian bursa to the peritoneal cavity, which is called the foramen of ovarian bursa. The ligament of ovarian bursa, which is the part of the mesosalpinx connecting the oviduct and uterus, surrounds the foramen of ovarian bursa. The ligament consists of a thick smooth muscle layer. The squares surrounded by dashed lines are magnified in the schema on the right side.

Supplementary Movie S1. Leakage of India ink from the ovarian bursa to extrabursa through the foramen of the ovarian bursa in C57BL/6N mouse at 3 months of age.

Supplementary Figure S2. The ratio of spleen weight to body weight in mice.

The strain-related difference in the same age is examined by the Kruskal-Wallis test followed by Scheffé's method. The differences between 3 and 6 months of age in the same strain is examined by the Mann-Whitney U-test. n = 5, 6 and 6 in B6, MRL/+ and MRL/lpr mice at 3 months of age and n = 4, 5 and 6 in B6, MRL/+ and MRL/lpr mice at 6 months of age. Data is presented as the mean ± SEM. $^{**}P < 0.01$

B6: C57BL/6N, MRL/+: MRL/MpJ, MRL/lpr: MRL/MpJ-Fas$^{lpr/lpr}$.

Figure 1

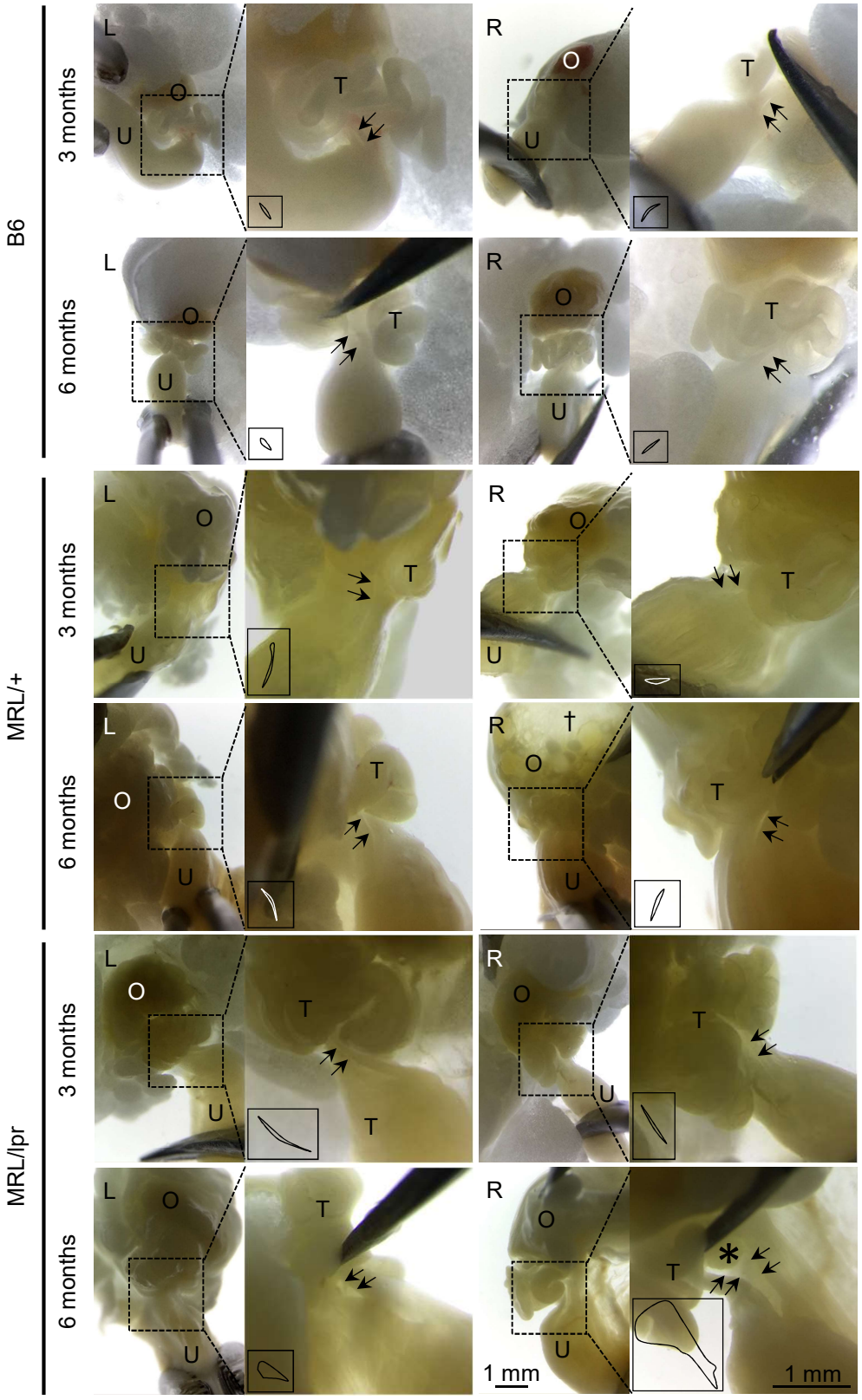

Figure 2

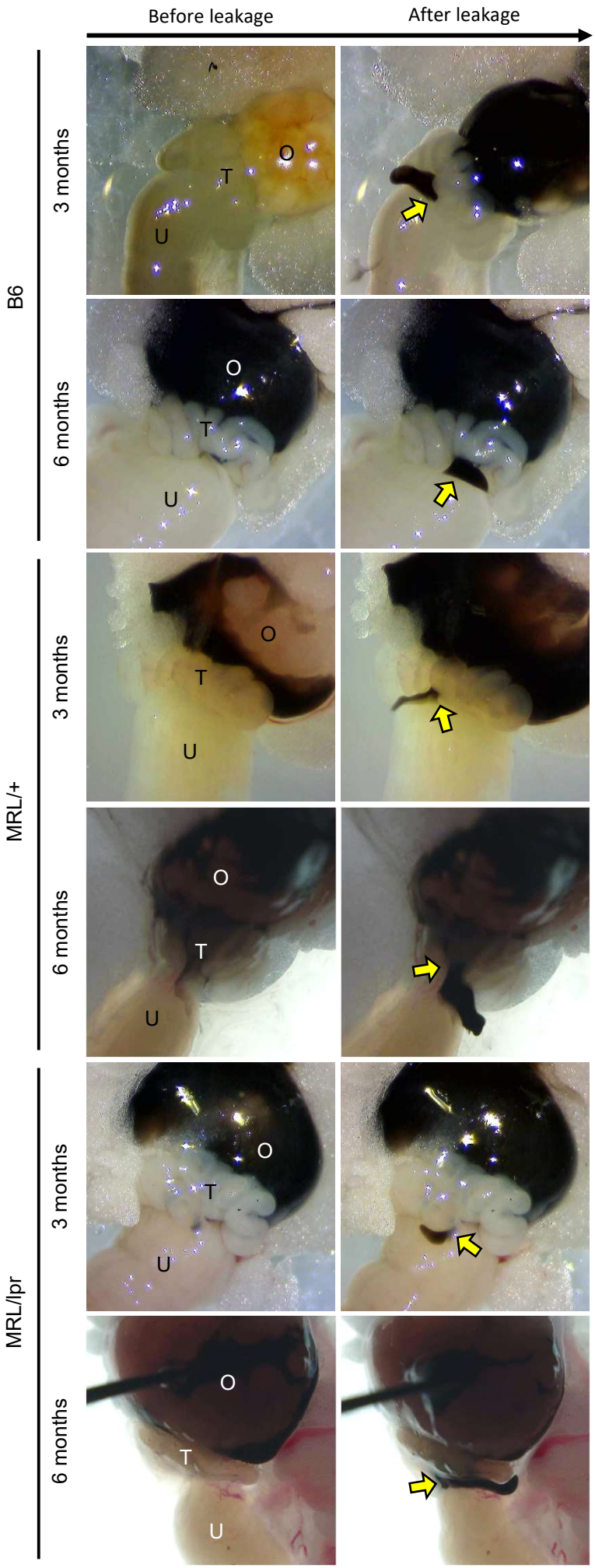
Before leakage
After leakage
B6
MRL/+
MRL/lpr
3 months
6 months
O
T
U

Figure 3

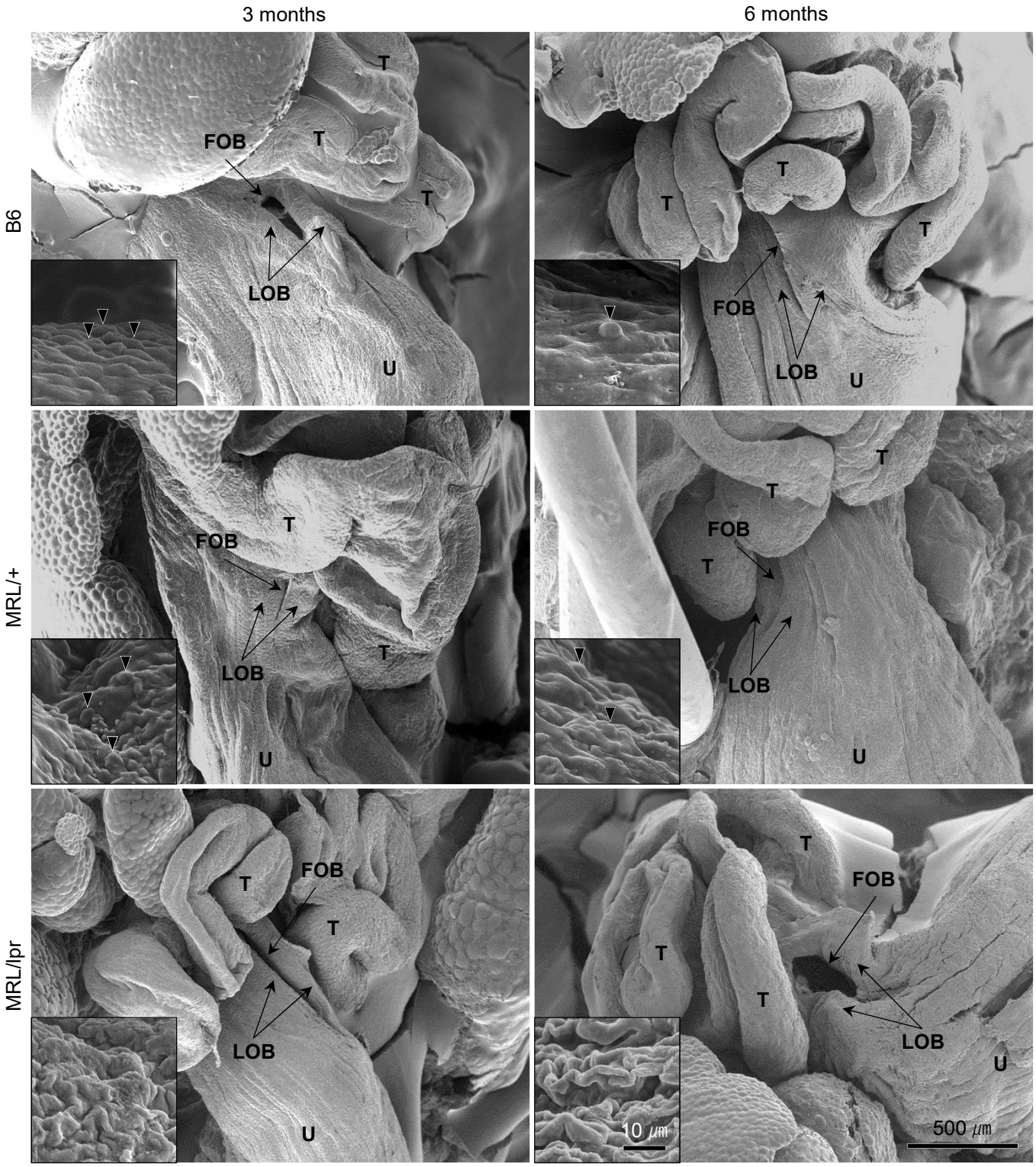

Figure 4

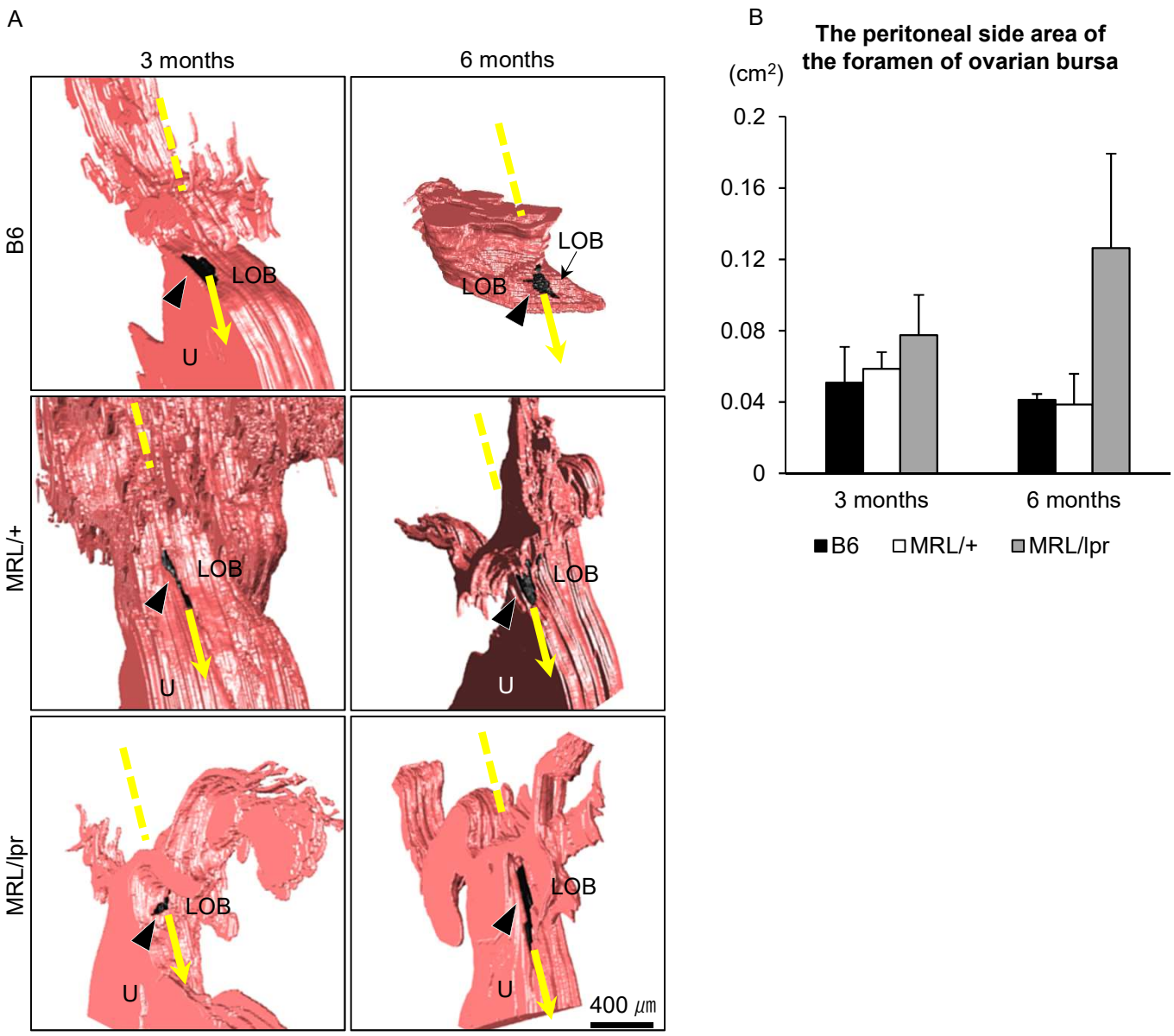
A
3 months
6 months
B6
MRL/+
MRL/lpr
LOB
U
400 μm
B
The peritoneal side area of the foramen of ovarian bursa
(cm²)
0.2
0.16
0.12
0.08
0.04
0
3 months
6 months
B6
MRL/+
MRL/lpr

Figure 5

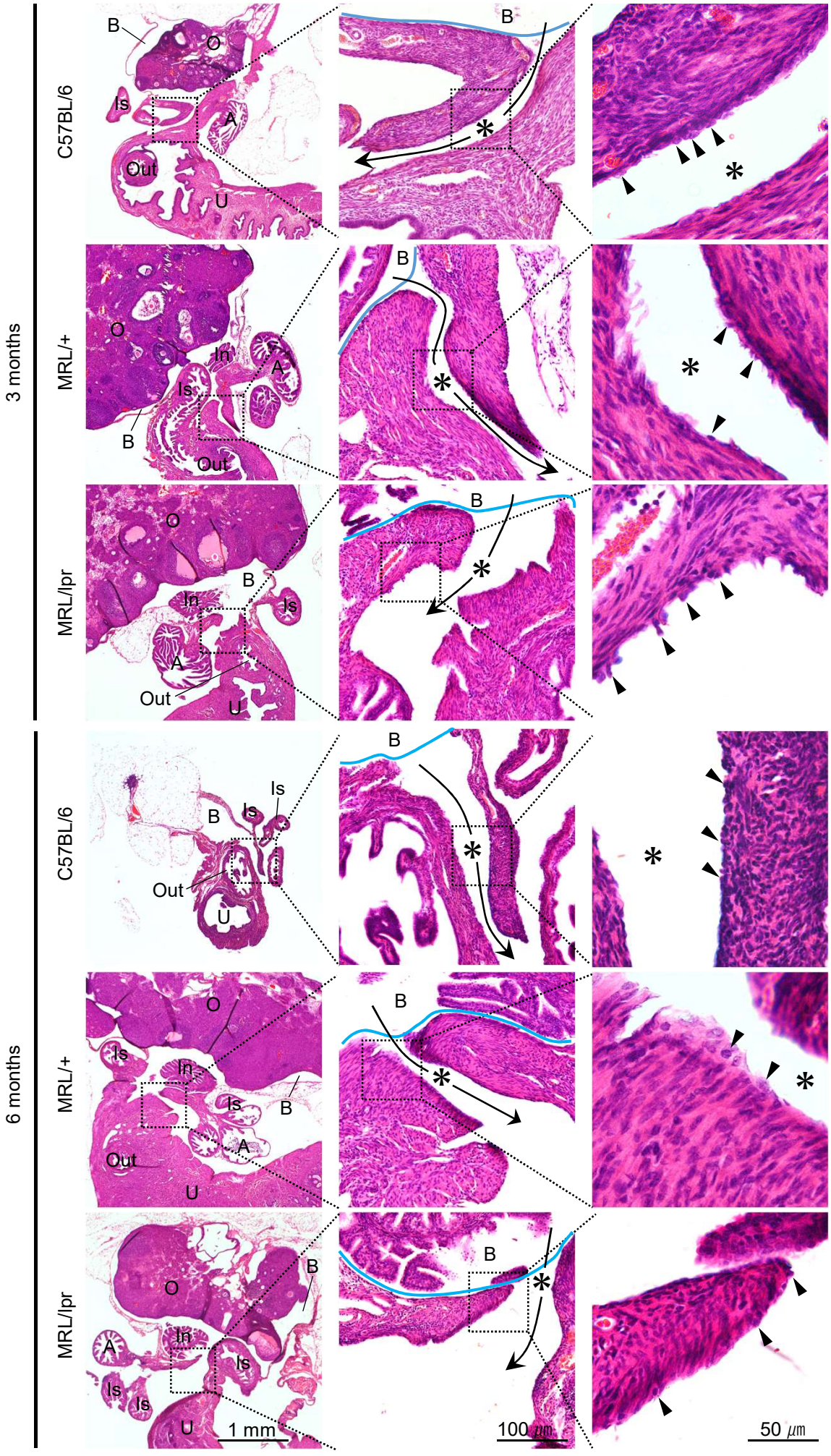
3 months
6 months
C57BL/6
MRL/+
MRL/lpr
B
O
Is
A
Out
U
In
1 mm
100 μm
50 μm

Figure 6

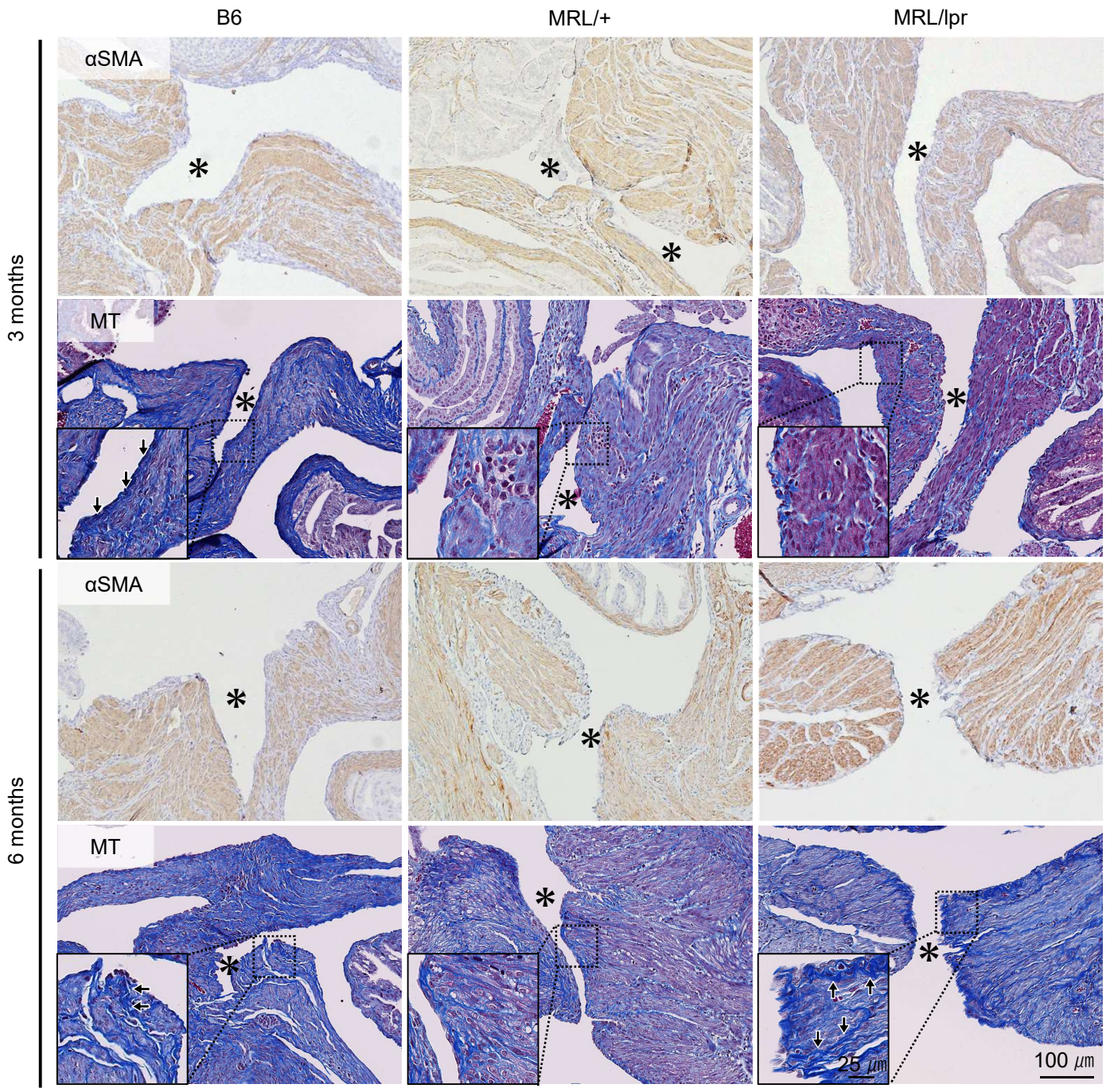

Figure 7

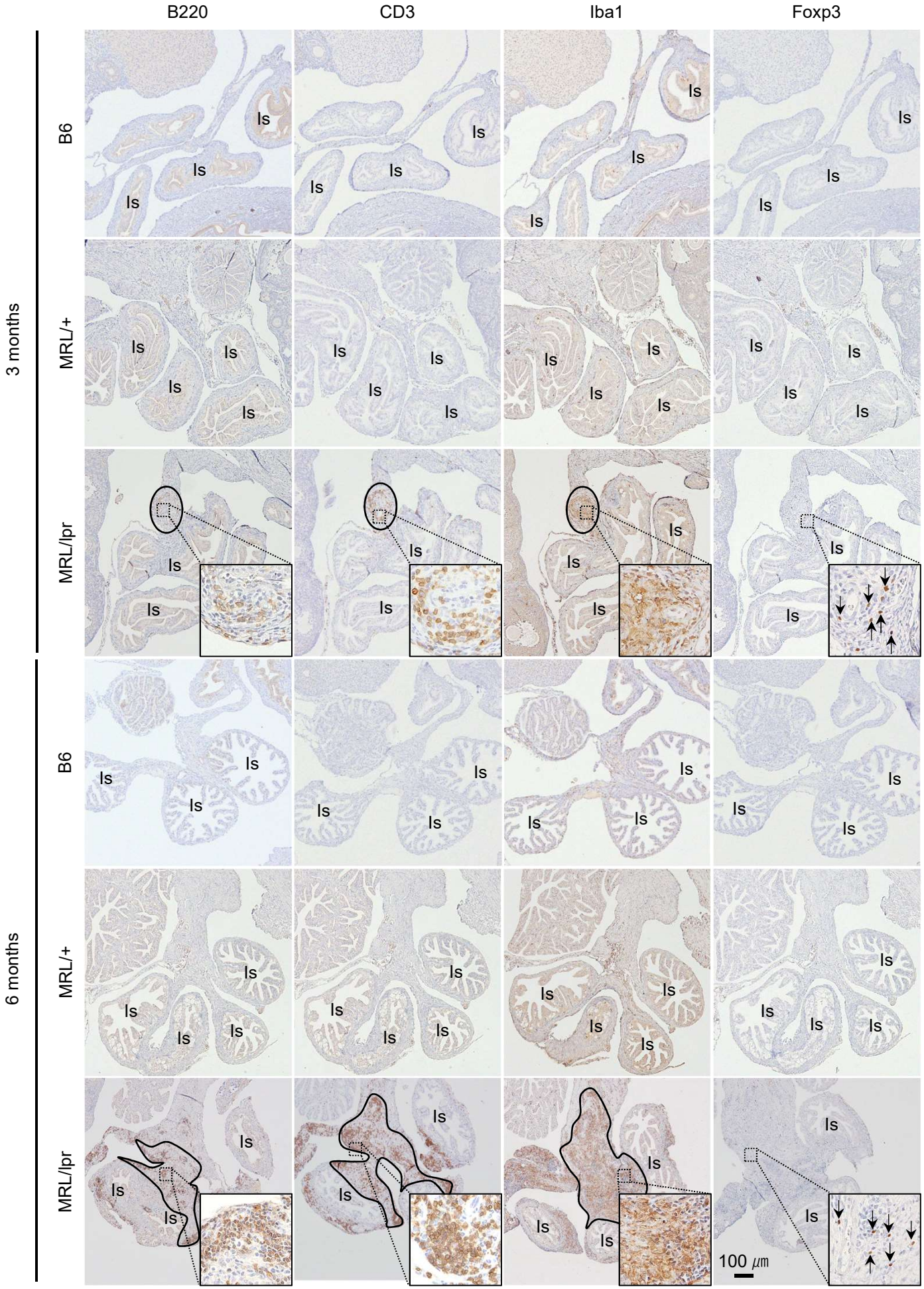

Figure 8

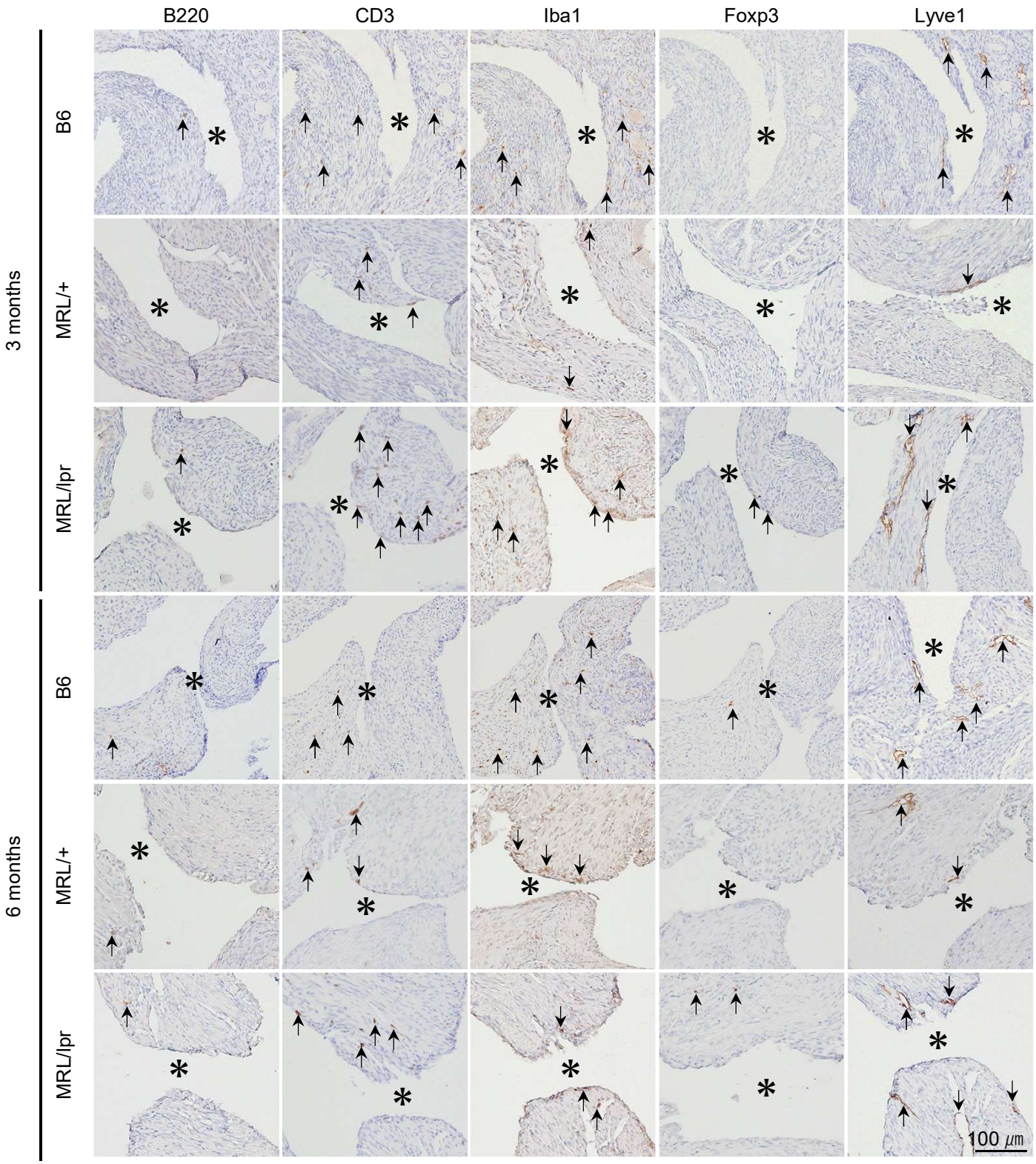
B220
CD3
Iba1
Foxp3
Lyve1
3 months
6 months
B6
MRL/+
MRL/lpr
B6
MRL/+
MRL/lpr
100 μm

Figure 9

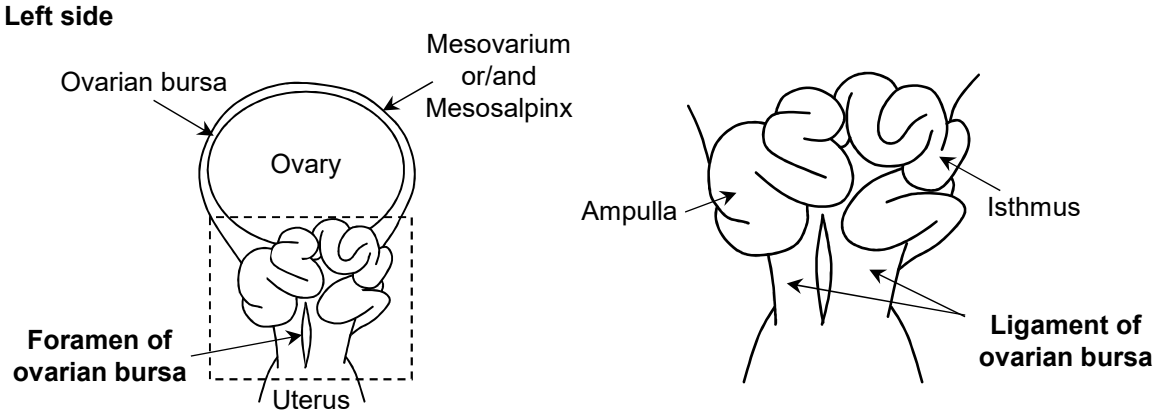
Left side
Ovarian bursa
Mesovarium
or/and
Mesosalpinx
Ovary
Foramen of
ovarian bursa
Uterus
Ampulla
Isthmus
Ligament of
ovarian bursa